Ultraviolet Photodissociation Dynamics of Cl_2 and $CFCl_3$ Adsorbed on Water Ice Surfaces

Akihiro Yabushita and Masahiro Kawasaki*

Graduate School of Global Environmental Studies and Department of Molecular Engineering, Kyoto University, Kyoto 606-8501, Japan

Shinri Sato

Catalysis Research Center and Graduate School of Environmental Earth Science, Hokkaido University, Sapporo 060-0811, Japan

Received: November 13, 2002; In Final Form: December 19, 2002

A difference in the UV photodissociation dynamics of chlorine and tricholorofluorocarbon has been observed when those molecules were adsorbed on water ice surfaces. This difference is mostly attributable to the difference in the interaction of the adsorbed molecule with surface water molecules of ice. In the photodissociation of Cl_2 at 300−414 nm, the branching ratios of the formation of $Cl^{\bullet}(^2P_{1/2})$ with respect to $Cl(^2P_{3/2})$ are different from those reported in the gas-phase photodissociation. However, in the photodissociation of $CFCl_3$ at 193 nm, the ratio is in good agreement with that reported in the gas-phase photodissociation. The kinetic energy distributions of the photofragment chlorine atoms reflect the interaction between the adsorbates and the surface water molecules.

Introduction

Chemistry on water ice films depends on the nature of interaction between adsorbed molecules and ice surfaces. The interactions of adsorbed molecules with the surfaces of amorphous and crystalline water ice films were investigated using thermal desorption spectroscopy (TDS), infrared absorption spectroscopy, and X-ray photoelectron spectroscopy[1,2] for carbon suboxide,[3] ozone,[4] thiophen,[5] cyanoacetylene,[6] chlorodifluoromethane,[7] ammonia,[8] and trichlorofluoromethane.[9] Theoretical calculations were carried out to study the interactions of small nonpolar compounds,[10] acetone and methanol,[11] hydrogen chloride, and hydrogen fluoride[12] with ice surfaces. The reactivity of ice surfaces toward certain molecules varies appreciably with phase and morphology of ice. Schaff and Roberts reported compounds possessing a functional group capable of accepting a hydrogen bond from the OH group of water ice show one or more thermal desorption states from an amorphous ice surface that are absent from crystalline ice.[2]

Photochemical reactions on ice have attracted attention because of their relevance in atmospheric processes.[13,14] Ice mediates chemical- and radiation-induced processes in interstellar, cometary, or planetary conditions.[15] In this paper, we have performed photodissociation of Cl_2 and $CFCl_3$ by measuring the translational energy distributions and the spin−orbit branching ratios of the $Cl(^2P_{3/2})$ and $Cl^*(^2P_{1/2})$ photofragments. The low-temperature study of the interaction of Cl_2 with water ice surfaces was reported by Banham et al.[16] The desorption temperature of Cl_2 from an water ice surface is 110 K. A TPD study for the interaction of Cl_2 with an amorphous ice surface was reported by Graham and Roberts.[17] They found that an exposure of 0.09 L at 100 K is sufficient to saturate the surface with Cl_2, because Cl_2 does not condense into Cl_2 multilayers at 100 K. Cl_2 desorbed mainly at 125 K. A secondary ion mass spectrometric measurement by Donsig et al. implied that Cl_2 reacts with ice above 130 K to form HOCl and HCl.[18] The interaction between a water ice surface and $CFCl_3$ has been investigated experimentally.[9,19] Horn et al. have studied the adsorption of $CFCl_3$ on the D_2O ice surface at 110 K using reflection−absorption infrared spectroscopy.[19] They conclude that $CFCl_3$ molecules are weakly and reversibly adsorbed onto the surface of ice film. According to Ogasawara et al. the bond between the ice surface and $CFCl_3$ is a hydrogen bond between chlorine and free OH.[9]

Experimental Section

Surface photodissociation of molecules adsorbed on crystalline and amorphous water ice surfaces was carried out in an ultrahigh vacuum chamber, which was equipped with two turbo molecular pumps in tandem, a pulsed molecular beam, an excimer laser, and a dye laser. The experimental details are described elsewhere.[20] In brief, ice films were prepared on polycrystalline Au substrates with (111) domains.[21] Two types of ice films were used in this experiment: porous amorphous solid water (P-ASW) and polycrystalline ice (PCI) films. The P-ASW film was grown by deposition of water on the polycrystalline Au substrate at 86−99 K with the backfilling method.[22−24] The PCI film was prepared by depositing water vapor at 130 K for 60 min and annealing for 25 min. The exposure was typically 1800 L (1 L = 1×10^{-6} Torr s), which resulted in the formation of 600 ML of H_2O on the Au substrate.[25] An amorphous ice film is characterized by the existence of free OH groups and the porosity of ice surface, while a crystalline ice film has grain boundaries.[20] The gas mixture of Cl_2 with N_2 diluent was introduced into a vacuum chamber and exposed with the backfilling method. $CFCl_3$ molecules without diluent was introduced into a vacuum chamber. The chamber pressure was 0.5×10^{-8} without sample molecule injection. From our previous experiment,[20] we supposed that Cl_2 or $CFCl_3$ formed a submonolayer on the ice films at 90 K after exposure of several L. Cl_2 was photodissociated at 300−414 nm with the YAG pumped dye laser (Lambda Physik, SCANmate, 1 mJ cm^{-2}

* Corresponding author. Fax: +81-75-753-5526. E-mail: kawasaki@photon.mbox.media.kyoto-u.ac.jp.

10.1021/jp027454y CCC: $25.00
Published on Web 02/14/2003

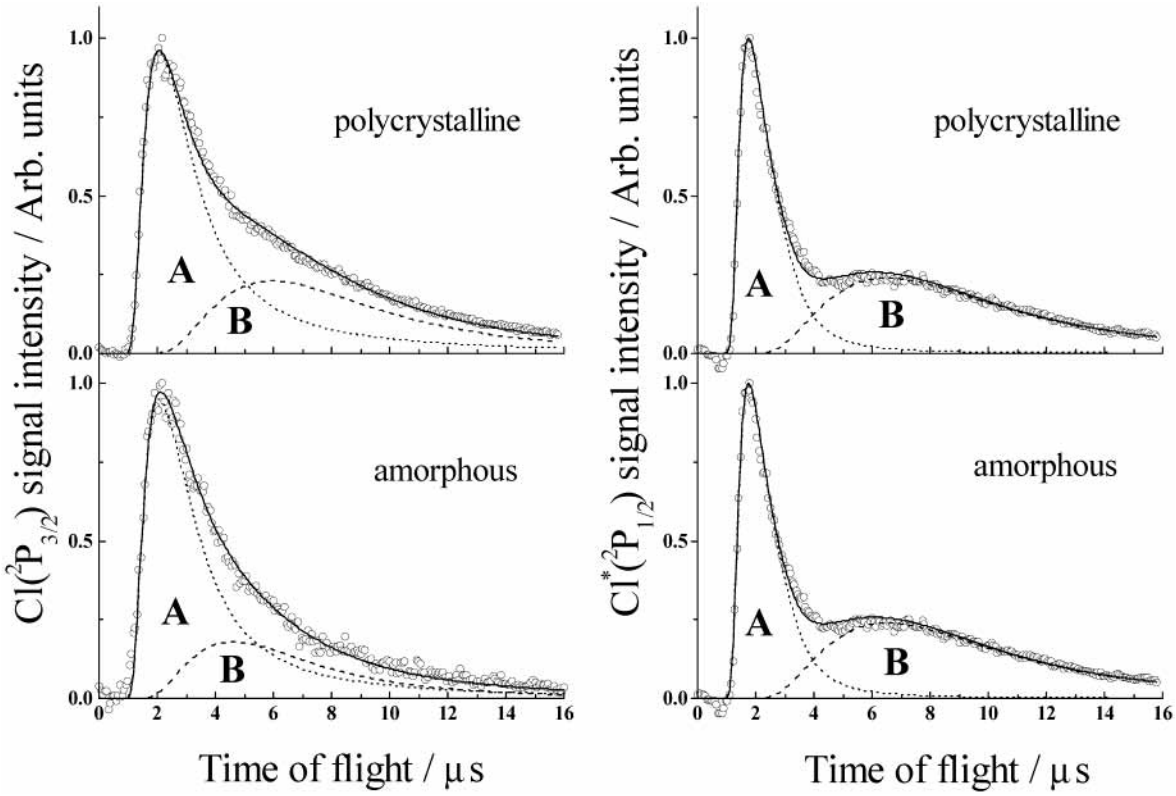

Figure 1. Time-of-flight spectra of $Cl(^2P_{3/2})$ and $Cl^*(^2P_{1/2})$ from the 193 nm photodissociation of $CFCl_3$ on a polycrystalline ice surface and an amorphous ice surface. Ice temperature $T = 90$ K, 1 L of $CFCl_3$. These spectra are resolved into two distributions: a Gaussian translational energy distribution marked by A with $\langle E_t\rangle_{Cl} = 0.42 \pm 0.02$ eV and $\langle E_t\rangle_{Cl^*} = 0.71 \pm 0.03$ eV for both amorphous and crystalline ice surfaces; a flux-weighted Maxwell−Boltzmann translational energy distribution marked by B with $T_{trans} = 540 \pm 50$ K for a crystalline ice surface and 1000 ± 50 K for an amorphous ice surface. The smooth solid curves correspond to the sum of these two distributions defined by eq 1. Details of curve fitting were described in ref 20.

pulse^{-1} at UV). $CFCl_3$ was photodissociated at 193 nm with an ArF excimer laser (Lambda Physik, COMPex, 10 Hz, typically reduced to 0.4 mJ cm^{-2} pulse^{-1} by optical filters). While the adsorbed molecules were photoirradiated, the sample molecule was slowly introduced accordingly, to keep amount of the adsorbate constant. Actually, the sample molecule was introduced through a leakage valve, typically in the effective pressure range of 10^{-9} Torr, to keep the signal intensity constant at a fixed time delay between photolysis and probe pulses. Another YAG pumped dye laser pulse (Lambda Physik, SCANmate, 0.2 mJ pulse^{-1} at UV) was used to ionize the photofragment by (2 + 1) resonance-enhanced multiphoton ionization (REMPI) at 235.336 nm for $Cl(^2P_{3/2})$ and 235.205 nm for $Cl^*(^2P_{1/2})$ with a lens ($f = 0.20$ m). For each spin−orbit state, the REMPI intensity, I, depends both on the quantum state population, N, and on the ionization efficiency. Thus, $I(Cl^*)/I(Cl) = [N(Cl^*)/N(Cl)]/f$. The scaling factor f was reported to be 1.06 ± 0.17 by Regan et al.[26] The subsequent REMPI signals of the chlorine atoms were detected by a time-of-flight mass spectrometer and normalized to the UV probe laser intensity. The distance, l, between the substrate and the detection region was varied from 3 to 5 mm to change the effective flight lengths for neutral photofragments, which was set typically to 3 mm. TOF spectra were taken as a function of time delay, t, between photolysis and probe pulses, which correspond to the flight time between the substrate and the detection region.

The TOF spectra were collected with the detector located along the surface normal. To simulate the obtained TOF spectra, we used a composite of normalized TOF functions, $S_G(t)$ and $S_{MB}(t)$. These functions correspond to a Gaussian translational energy distribution $P_G(E_t)$ and a flux-weighted Maxwell−Boltzmann translational energy distributions $P_{MB}(E_t)$, respectively. $P_G(E_t)$ is characterized by the average energy, $\langle E_t\rangle$, and the energy width, w. $P_{MB}(E_t)$ is characterized by the average kinetic energy $\langle E_t\rangle = 2k_BT_{trans}$ where k_B is the Boltzmann constant and T_{trans} is the translational temperature. Conversion from the energy distribution to the time-of-flight distribution was performed using the Jacobian listed by Zimmerman and Ho.[27] The details of the simulation of the TOF spectra were described in our previous paper.[20]

$$S(C, t) = CS_G(t) + (1 - C)S_{MB}(t) \quad (1)$$

$$P_G(E_t) = [w(2\pi)^{1/2}]^{-1} \exp[-2(E_t - \langle E_t\rangle)^2/w^2] \quad (2)$$

$$P_{MB}(E_t) = (k_BT_{trans})^{-2}E_t \exp[-E_t/(k_BT_{trans})] \quad (3)$$

where C is a coefficient, and t is the time-of-flight of the photofragments.

Results

Photodissociation of $CFCl_3$ on Water Ice Surfaces at 193 nm. Cl and Cl* photofragments from the 193 nm photodissociation of $CFCl_3$ adsorbed on amorphous and crystalline water ice surfaces were observed, which have both fast and slow components. Typical TOF spectra are shown in Figure 1. Solid curves are a best-fit $S(C, t)$ of eq 1. The fast component (channel A) is a Gaussian distribution. The slow one (channel B) is a flux-weighted Maxwell−Boltzmann distribution. Both Cl and Cl* photofragments have the same threshold TOF of 0.80 ± 0.05 μs. On the assumption that the angular distribution of the

TABLE 1: Average Translational Energies of $Cl(^2P_{3/2})$ and $Cl^*(^2P_{1/2})$ Photofragments from $CFCl_3$ and Cl_2 Adsorbed on Ice Surfaces

		Gaussian distribution for Channel A		Maxwell−Boltzmann distribution for Channel B		
parent molecule	detected species	average energy[a] (eV)	coefficient C[a]	average energy[a] (eV)	translational temperature[a] (K)	coefficient C [a]
$CFCl_3$	Cl	0.42 ± 0.02	0.65 ± 0.07	0.17 ± 0.01 (P-ASW)[b] 0.09 ± 0.01 (PCI)[c]	1000 ± 50 (P-ASW) 540 ± 50 (PCI)	0.35 ± 0.07
	Cl^*	0.71 ± 0.03	0.49 ± 0.07	0.17 ± 0.01 (P-ASW) 0.09 ± 0.01 (PCI)	1000 ± 50 (P-ASW) 540 ± 50 (PCI)	0.51 ± 0.07
Cl_2	Cl	0.38 ± 0.04	0.65 ± 0.05	0.13 ± 0.01	770 ± 40	0.35 ± 0.05
	Cl^*	0.48 ± 0.04	0.87 ± 0.02	0.13 ± 0.01	770 ± 40	0.13 ± 0.02

[a] Average energy, translational temperature and coefficient appear in eq 1. [b] P-ASW stands for porous amorphous solid water ice surface. [c] PCI stands for polycrystalline ice surface.

TABLE 2: Branching Ratios of $Cl^*(^2P_{1/2})$ and $Cl(^2P_{3/2})$ from Photodissociation of $CFCl_3$ and Cl_2 on a Polycrystalline Ice Surface and in the Gas Phase

		ice surface		
adsorbate	wavelength (nm)	$I(Cl^*)/I(Cl)$[a]	$N(Cl^*)/N(Cl)$[b]	gas phase
$CFCl_3$	193	0.24 ± 0.02	0.25 ± 0.02	0.30[c]
Cl_2	300	0.20 ± 0.03	0.30 ± 0.05	0[d]
	325	0.19 ± 0.02	0.29 ± 0.03	0[d]
	351	0.19 ± 0.01	0.29 ± 0.02	0.003[d]
	400	0.16 ± 0.01	0.24 ± 0.02	0.43[d]
	414	0.10 ± 0.01	0.15 ± 0.02	0.66[d]

[a] Experimental signal intensity ratio. [b] Population ratio after correction for detection efficiency and electronic relaxation; see text for details. [c] From ref 38. [d] From ref 29.

photofragments from the substrate is a function of $\cos^n\theta$, where θ is the desorption polar angle, the best fitting value of the exponent (n) for the TOF spectra was decided to be 2 for channel A. The Gaussian distribution for Cl is characterized by $\langle E_t\rangle_{Cl} = 0.42 \pm 0.02$ eV, and $w = 0.91 \pm 0.09$ eV, for both amorphous and crystalline ice. For Cl^*, $\langle E_t\rangle_{Cl^*}$ is 0.71 ± 0.03 eV and $w = 0.65 \pm 0.06$ eV. For the slow Maxwell−Boltzmann distribution, $n = 0$ was adopted for the angular distribution. The energy distribution is characterized by $2k_BT_{trans} = 0.09 \pm 0.01$ eV (540 ± 50 K) for crystalline ice, and $2k_BT_{trans} = 0.17 \pm 0.01$ eV (1000 ± 50 K) for amorphous ice. These translational energy parameters $\langle E_t\rangle$ and $2k_BT_{trans}$ were found to be independent of photolysis laser intensity for 0.1−1 mJ cm^{-2} $pulse^{-1}$ and under an exposure of 1 L.

The contributions of channel B to the total TOF spectra of Cl on amorphous and crystalline ice are 35 ± 7%, while that for Cl^* is 51 ± 7%. Table 1 summarizes these results for the energy distributions.

The time-integrated TOF signal intensity ratios $I(Cl^*)/I(Cl)$ were 0.24 ± 0.02 for both amorphous and crystalline ice surfaces. After correction for the relative sensitivity of the each REMPI transition, the ratio of the quantum state population is $N(Cl^*)/N(Cl) = 0.25 \pm 0.02$, which is close to the ratio observed in the gas-phase photodissociation at 193 nm (Table 2). Because of the weak interaction, no spectral shift is expected. When we performed the photodissociation at 248 nm as a reference experiment, no Cl signals were observed due to the small absorption cross section, which is below 10^{-22} cm^2 in the gas phase.

Photodissociation of Cl_2 on Water Ice Surfaces at 300−414 nm. The TOF spectra of Cl and Cl^* atoms from the photodissociation of Cl_2 on water ice surfaces are essentially the same as those described previously.[20] Figure 2 shows typical TOF spectra, $S(C, t)$, of Cl and Cl^* atoms from the 351 nm photodissociation of Cl_2. The exponent $n = 2$ for the angular distribution of the photofragments was adopted for channel A according to Giorgi et al.[28] The Gaussian distribution of Cl is characterized by $\langle E_t\rangle_{Cl} = 0.38 \pm 0.02$ eV and $w = 0.37 \pm 0.02$ eV for both amorphous and crystalline ice. $\langle E_t\rangle_{Cl^*}$ is 0.48 ± 0.02 eV and $w = 0.37 \pm 0.02$ eV. The average energies of channel B, $2k_BT_{trans}$, are 0.13 ± 0.01 eV for Cl and Cl^*. These translational energy parameters $\langle E_t\rangle$ and $2k_BT_{trans}$ were found to be independent of photolysis laser intensity up to 5 mJ cm^{-2} $pulse^{-1}$, under an exposure of 1 L and the states of ice surfaces (amorphous or crystalline).

The time-integrated TOF signal intensity ratios $I(Cl^*)/I(Cl)$ on polycrystalline ice surface at 300−414 nm are almost independent of the dissociation wavelengths as shown in Table 2. In the TOF spectra, the Cl atoms have an appreciable portion of the slow component in their broad TOF distributions while the Cl^* atoms have only a limited portion of this component in their narrow TOF distributions. The contributions of channel B to the total TOF spectra of Cl on amorphous and crystalline ice are 35 ± 5%, while that for Cl^* is 13 ± 2%. We assumed that (a) the contribution of channel B should be the same for both Cl^* and Cl, and (b) the electronically excited-state Cl^* atoms are internally relaxed to the ground-state Cl atom. Based on this assumption and after correction for the relative sensitivities, the population ratios, $N(Cl^*)/N(Cl)$, are listed in Table 2, which are different from those reported in the gas-phase photodissociation.[29]

Effects of the States of Water Ice Surfaces on Cl Photofragment Yields and Photodissociation Cross Sections. The Cl signal intensity from the photodissociation of $CFCl_3$ was 6 ± 2 times weaker on P-ASW than on PCI under the same exposure conditions, and that of Cl_2 was about 10 times weaker. For measurement of the relative photodissociation cross sections of $CFCl_3$ or Cl_2 on amorphous and crystalline ice surfaces, the decay curve of the Cl signal intensity was measured as a function of irradiation time after the sample molecules were once exposed on ice surfaces at 90 K under 1 L condition.

Since the photodissociation process follows a single exponential law, eq 4 determines the photodissociation cross section, σ_{diss}.

$$N = N_0 \exp(-\sigma_{diss} n_{h\nu}) \tag{4}$$

where N is the residual amount of the sample molecules on an ice surface, N_0 the initial amount of the sample molecules, and $n_{h\nu}$ the number of photons irradiated.[30] From the initial part of the slopes of these curves, we derived σ_{diss}, or the absorption cross section σ_{abs} times dissociation quantum yield ϕ; σ_{diss}(P-ASW)/σ_{diss}(PCI) = σ_{abs}(P-ASW)ϕ(P-ASW)/σ_{abs}(PCI)ϕ(PCI) = 1.2 for $CFCl_3$, and 0.15 for Cl_2.

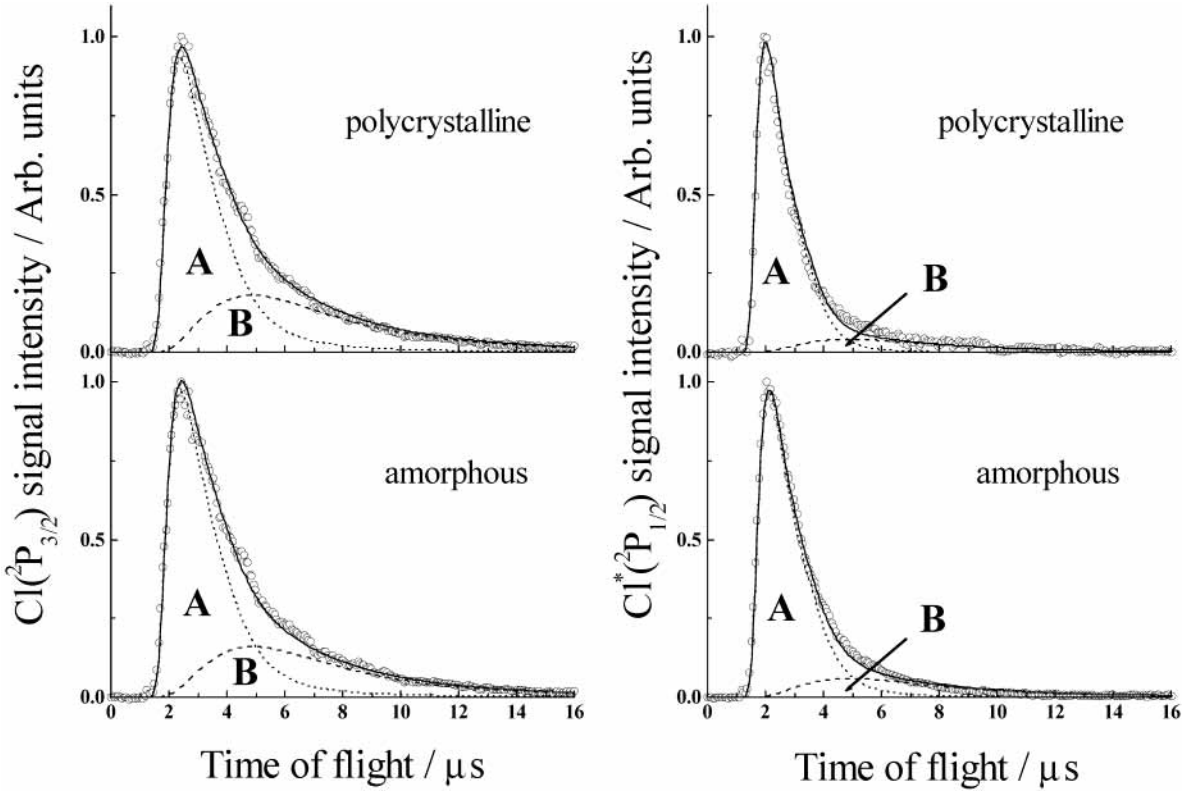

Figure 2. Time-of-flight spectra of $Cl(^2P_{3/2})$ and $Cl^*(^2P_{1/2})$ from the 351 nm photodissociation of Cl_2 on a crystalline ice surface and an amorphous ice surface. Ice temperature $T = 86$ K, 1 L of Cl_2 for crystalline and amorphous ice surfaces. Gaussian translational energy distribution marked by A is characterized with $\langle E_t \rangle_{Cl} = 0.38 \pm 0.04$ eV, and a flux-weighted Maxwell−Boltzmann translational energy distribution marked by B with $T_{trans} = 770 \pm 40$ K. The smooth solid curves are the sum of these two distributions. The TOF spectra for $Cl^*(^2P_{1/2})$, which consist mostly of channel A with $\langle E_t \rangle_{Cl^*} = 0.48 \pm 0.04$ eV.

Photodissociation of HCl on Water Ice Sufaces at 193 nm. As a reference experiment, the ice surface at 89−93 K was exposed with a mixture gas of HCl and N_2 up to a few Langmuir exposure, and then, was irradiated at 193 nm. No REMPI signal of chlorine atoms was observed. The interaction between HCl and ice is completely different from that for Cl_2 and $CFCl_3$.[31−33] By using a combination of the infrared transmission spectroscopy and Monte Carlo ab initio simulations, Devlin et al. reported that HCl dissolves into ice layers to form $H^+ + Cl^-$ at the surface of ice film even at 50 K.[32] Near 90 K, the formation of contact hydronium−chloride ion pairs abruptly occurs, resulting in an ionic hydrate layer rich in Zundel cations.[34] Thus, no photodissociation of HCl occurred on the ice surface at 89−93 K.

Discussion

Photodissociation Mechanisms of $CFCl_3$ on Water Ice Surfaces. The photodissociation of $CFCl_3$ at 193 nm in the gas phase leads to the following reaction with a nonthermal translational energy distribution for the photofragments:[35]

$$CFCl_3 + h\nu \rightarrow CFCl_2 + Cl \qquad (5)$$

At higher laser fluence a fraction of the nascent $CFCl_2$ radicals absorbs a further photon and dissociates into CFCl + Cl in the gas phase. In the present experiment, since ArF laser fluence is less than 0.4 mJ cm^{-2} $pulse^{-1}$, this secondary process does not occur. Therefore, reaction 5 is the dominant primary process. The UV photodecomposition of $CFCl_3$ on an ice surface was studied by Ogasawara and Kawai.[9] They reported no IR absorption peaks assignable to adsorbed $CFCl_2$ in IRAS during the irradiation with 193 nm light. Because $CFCl_3$ is weakly and reversibly adsorbed onto the surface of ice film, the $CFCl_2$ fragment was removed from the surface immediately after photodecomposition.[19]

Based on the thermodynamic data, $D_0(CFCl_2-Cl) = 3.25$ eV, the maximum available energy for the 193 nm photodissociation would be 3.17 eV. In the present experiment, the maximum translational energy of the Cl photofragment, $E_t^{max}(Cl) = 2.6 \pm 0.3$ eV from the threshold TOF gives the maximum center-of-mass translational energy, E_t^{max} (Cl + $CFCl_2$) $= 3.5 \pm 0.4$ eV, which is in fair agreement with the calculated maximum available energy. Thus, the fast TOF component with the Gaussian distribution could be attributable to the direct photodissociation of $CFCl_3$ on the ice surface. In the gas phase, the average kinetic energy of the product chlorine atoms from the photodissociation of $CFCl_3$ at around 190 nm was reported to be 1.0 eV.[35,36] Based on the average translational energies $\langle E_t \rangle$ of Table 1, the energy relaxation of the chlorine photofragments is efficient on the ice surface. Due to rapid energy flow to ice, some of chlorine photofragments from the photodissociation of $CFCl_3$ are translationally relaxed by surface water molecules. Thus, the average kinetic energy $\langle E_t \rangle$ of channel A is lower than that in the gas phase. The discrepancy with $\langle E_t \rangle_{Cl} - \langle E_t \rangle_{Cl^*}$ could be due to the fact that the Cl channel deposits a greater fraction of available energy in $CFCl_2$ internal excitation.[37,38]

For Channel B processes, flux-weighted Maxwell−Boltzmann distributions with $2k_BT_{trans} = 0.09 \pm 0.01$ eV for PCI and 0.17 $\pm$ 0.01 eV for P-ASW were observed. This process is attributed to the photofragment atoms that have translationally relaxed by collisions with water ice molecules and/or other $CFCl_3$ molecules.

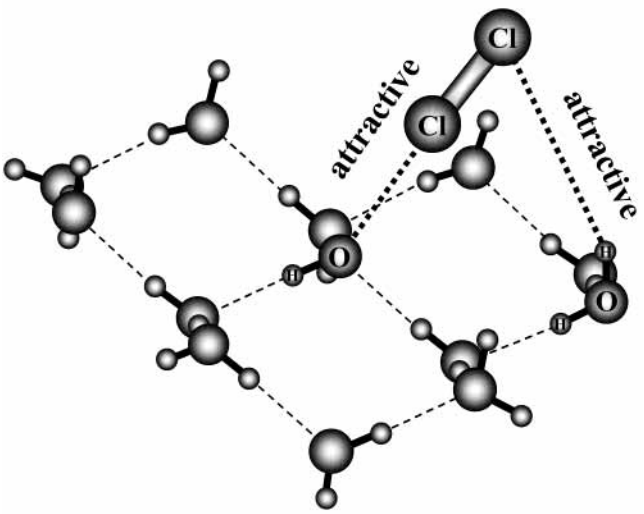

Figure 3. A schematic diagram of a chlorine molecule adsorbed on the surface water molecules after a theoretical calculation by Bianco.[42] The interaction between Cl_2 and H_2O is attractive while that between Cl_2 molecules is repulsive.

We examined the polarization dependent yields of Cl in channel A with s- and p-polarized dissociation laser light for PCI. Supposing $CFCl_3$ is randomly oriented on the ice surface, the theoretically calculated polarization ratio is $I_s/I_p = 4/3$. This ratio is close to what we observed, $I_s/I_p = 1.4 \pm 0.2$. Therefore, orientation of $CFCl_3$ on the ice surface is likely to be random.

The branching ratios $[Cl^*]/[Cl]$ from the 193 nm photodissociation of $CFCl_3$ on the ice surfaces are essentially the same as that in the gas phase. The interaction of $CFCl_3$ with the ice surface is so limited that the electronic structure of the molecule is not affected by adsorption on ice. In fact, the solubility of $CFCl_3$ in water is 0.0086 mol kg^{-1} bar^{-1}, which is much lower than 0.095 mol kg^{-1} bar^{-1} for Cl_2.[39,40]

Photodissociation Mechanisms of Cl_2 on Water Ice Surfaces. Adsorption states of Cl_2 on ice surfaces have been described in our previous paper.[20] The polarization ratio I_s/I_p was 1.2 ± 0.1 for PCI. Therefore, orientation of Cl_2 on the ice surface is likely to be random.

Based on the thermodynamic data, $D_0(Cl-Cl) = 2.475$ eV, the maximum available energy for the 351 nm photodissociation would be 1.1 eV. The interaction energy for $Cl_2\cdots(OH_2)_4$ is 0.12 ± 0.01 eV.[41] The maximum translational energy for each Cl atom is calculated to be $E_t^{max} = (h\nu - D_0 - 0.12)/2 = 0.46$ eV. This value is close to the average energy we observed for channel A, that is, 0.38 ± 0.04 eV for Cl, and 0.48 ± 0.04 eV for Cl^*. Thus, channel A could be attributable to the direct photodissociation of Cl_2 on the ice surface.

According to a theoretical calculation by Bianco,[42] Cl_2 molecules adsorbed on the surface water molecules do not nucleate due to repulsive force between Cl_2 molecules, as depicted in Figure 3. Actually Cl_2 does not condense into Cl_2 multilayers at 100 K.[17] The hydrolysis of molecular chlorine and its reverse reaction have been studied by ab initio molecular dynamics.[43] The hydrolysis reaction involves Cl_2 and H_2O molecules to produce solvated chlorine and hydrogen ions. Static secondary ion mass spectrometry measurements reported by Donsig et al. imply that Cl_2 reacts with ice above 130 K to form HOCl and HCl.[18] Therefore, Cl_2 strongly interacts with water molecules of the ice surface. The solubility of Cl_2 in water is much larger than that of $CFCl_3$.[39,40] Hence, the reaction dynamics differs from that for $CFCl_3$.

The Interaction between Ice and Molecules. Sadtchenko et al. reported that CCl_4 adsorption on ice prepared at 130 K results in the formation of metastable two-dimensional islands, while CCl_4 adsorption on ice prepared at 95 K proceeds through formation of three-dimensional clusters in the pores of microscopically rough ice.[44] $CFCl_3$ is likely to have the similar nature to CCl_4 on an ice surface.[19] Based on the study for CCl_4, it is likely that $CFCl_3$ adsorbed on the ice surface can nucleate. Therefore, $CFCl_3$ photoprepared at 193 nm is electronically quenched efficiently. The photofragments from the photodissociation of isolated $CFCl_3$ adsorbed on the ice surface are mostly detected. Hence, the photodissociation dynamics resemble that in the gas phase and the ratios σ_{abs}(P-ASW)/σ_{abs}(PCI) and ϕ(P-ASW)/ϕ(PCI) are considered to be close to unity. Actually the ratio σ_{abs}(P-ASW)ϕ(P-ASW)/σ_{abs}(PCI)ϕ(PCI) was 1.2. However, under the same exposure condition of $CFCl_3$ on the higher porous ice surface (P-ASW) or the lower porous ice surface (PCI), the Cl signal intensity from the photodissociation was weaker on the P-ASW surface than the PCI surface. This can be explained by assuming that the nucleation occurs more heavily on P-ASW than PCI, that is, the electronic quenching is more efficient on P-ASW than on PCI.

According to Geiger et al.[41] and Bianco,[42] Cl_2 molecules on the ice surface interact with water with attractive force of the order of 0.1 eV. Due to the repulsion force between Cl_2, nucleation cannot occur.[17] Hence, the electronic quenching of the photoprepared Cl_2 by neighbor Cl_2 would not occur. In our experiment, the Cl signal intensity from the photodissociation was weaker on the P-ASW surface than the PCI surface, and also the ratio σ_{abs}(P-ASW)ϕ(P-ASW)/σ_{abs}(PCI)ϕ(PCI) was 0.15. Photoprepared Cl_2 is more rapidly electronically quenched on the P-ASW surface than on the PCI surface due to the interaction between Cl_2 and the surface water. In other words, the ratio ϕ(P-ASW)/ϕ(PCI) is much less than unity because the surface OH groups are more abundant on P-ASW than PCI, which interact with Cl_2. Hence, the photodissociation dynamics on ice is different from that in the gas phase.

Adiabaticity of Cl_2 Potential Curves. The Cl_2−water complex, Cl_2-H_2O, has a dipole moment of 0.24 D, and Cl_2-3H_2O has that of 0.54 D, which are calculated by Bianco at the MP2 level of theory using effective core potentials for all the heavy atoms.[42] The bond length of Cl_2 (2.011 Å in the isolated molecule) is enlongated to 2.037 Å for Cl_2-3H_2O.[42] Since the interaction of the adsorbed Cl_2 with H_2O is relatively strong and the potential curves are strongly distorted, adiabaticities of the Cl_2 potential curves change so much that the spin−orbit branching ratios of the $Cl(^2P_{3/2})$ and $Cl^*(^2P_{1/2})$ photofragments are different from those of the isolated molecules.

When Cl_2 absorbs a UV photon, it dissociates through either the parallel or perpendicular transitions:

$$Cl_2 + h\nu \rightarrow Cl_2(B^3\Pi_u, \Omega = 0^+) \rightarrow Cl(^2P_{3/2}) + Cl^*(^2P_{1/2}) \quad (6)$$

$$Cl_2 + h\nu \rightarrow Cl_2(C^1\Pi_u, \Omega = 1) \rightarrow Cl(^2P_{3/2}) + Cl(^2P_{3/2}) \quad (7)$$

Gaseous Cl_2 has an absorption continuum in the region of 300−400 nm and weak absorption at $\lambda < 250$ nm. The absorption spectrum at 351 nm is dominated (99%) by the C $1_u(^1\Pi_u)$ state that is correlated with the formation of two Cl atoms, while the $0_u^+(B\ ^3\Pi_u)$ state which produces one Cl^* and one Cl contributes to photoabsorption less than 1%.[29,45] The Cl^*/Cl branching ratio, following gas-phase photolysis of Cl_2, has been extensively measured in the region 310−470 nm and results show variation

in the dissociation wavelength. Samartzis et al. reported the branching ratios for the Cl_2 photodissociation at 310−470 nm.[29] Their branching ratios $N(Cl^*)/N(Cl)$ at 300, 325, 351, 400, and 414 nm, are 0, 0, 0.003, 0.43, and 0.66, respectively. However, those on PCI at the corresponding wavelengths are 0.30, 0.29, 0.29, 0.24, and 0.15, respectively (Table 2).

The nuclear kinetic energy operator gives rise to a nonadiabatic interaction on the adiabatic potential.[46] The Rosen-Zener-Demkov (RZD) type nonadiabatic transition from the C $^1\Pi_u$ state to the third 1_u ($^3\Sigma^+_{1u}$) state of Cl_2 that is correlated adiabatically with $Cl + Cl^*$ is responsible for the production of Cl^*.[47,48] The photodissociation wavelength dependence of the product branching ratio $N(Cl^*)/N(Cl)$ depends on the degree of interaction of the potential curve.[29] The ratios in the gas phase are well reproduced by the RZD transition mechanism.

The 330 nm absorption band of the adsorbed chlorine is expected to be shifted only slightly toward shorter wavelength from an analogy with bromine and iodine water complexes.[49] Thus, the UV Franck−Condon region for Cl_2 on ice is not affected by the interaction with ice. The interaction of the adsorbed Cl_2 with H_2O is relatively strong at the asymptotic region of the potential curves. Potential energies rise at the longer internuclear distances. Thus, the degree of the RZD interaction between the electronically excited potential curves of Cl_2 on ice could be similar even though the photoprepared state is different at different UV wavelength. In other words, the product branching ratios $N(Cl^*)/N(Cl)$ become almost independent of the positions of Franck−Condon excitation (or the initial excitation position of the potential curves), but depend solely on the RZD interaction at longer internuclear distances.

Conclusion

Cl_2 and $CFCl_3$ are adsorbed at 86−99 K on two different states of ice surfaces, porous amorphous solid water (P-ASW) and polycrystalline ice (PCI). $Cl(^2P_{3/2})$ and $Cl^*(^2P_{1/2})$ photofragments have been measured to investigate the dissociation mechanisms of Cl_2 at 300−414 nm and $CFCl_3$ at 193 nm as a function of photolysis laser intensity, coverage of the adsorbates, and the states of the ice surfaces. The kinetic energy distributions of the chlorine atom photofragments are explained by a combination of the direct photodissociation process and relaxation processes. For $CFCl_3$ the absorption cross sections were similar on both P-ASW and PCI surfaces. The relative quantum yield for the formation of Cl on P-ASW is, however, weaker less than on PCI by an order of magnitude. The electronic quenching occurs efficiently for $CFCl_3$ due to nucleation of the adsorbates. The spin−orbit branching ratio of the $Cl(^2P_{3/2})$ and $Cl^*(^2P_{1/2})$ photofragments on PCI is essentially the same as that in the gas-phase photodissociation, suggesting a weak interaction of $CFCl_3$ with surface water molecules. For Cl_2, the branching ratios at 300−414 nm are completely different from those reported in the gas-phase photodissociation. Along with those results, the fact that the signal intensity on P-ASW is weaker than on PCI by an order of magnitude suggests a relatively strong interaction between chlorine molecules and the OH groups of the surface water molecules on P-ASW.

Acknowledgment. The authors thank Mr. A. Yane for his help in experiment. Discussion with Profs. M. N. R. Ashfold, R. Bianco, S. Yabushita, and H. Tachikawa is appreciated. This work is supported by a Grant-in-Aid in the priority field "Radical chain reactions" from the Ministry of Education of Japan.

References and Notes

(1) Schaff, J. E.; Roberts, J. T. *Surf. Sci.* **1999**, *426*, 384.
(2) Schaff, J. E.; Roberts, J. T. *J. Phys. Chem.* **1996**, *100*, 14151.
(3) Couturier-Tamburelli, I.; Chiavassa, T.; Pourcin, J. *J. Phys. Chem. B* **1999**, *103*, 3677.
(4) Chaabouni, H.; Schriver-Mazzuoli, L.; Schriver, A. *J. Phys. Chem. A* **2000**, *104*, 6962.
(5) Haberkern, H.; Haq, S.; Swiderek, P. *Surf. Sci.* **2001**, *490*, 160.
(6) Borget, F.; Chiavassa, T.; Allouche, A.; Marinelli, F.; Aycard, J. *J. Phys. Chem. A* **2000**, *104*, 6962.
(7) Safarik, D. J.; Meyer, R. J.; Mullins, C. B. *J. Vac. Sci. Technol. A* **2001**, *19*, 1537.
(8) Ogasawara, H.; Horimoto, N.; Kawai, M. *J. Chem. Phys.* **2000**, *112*, 8229.
(9) Ogasawara, H.; Kawai, M. *Surf. Sci.* **2002**, *502*−*503*, 285.
(10) Monca, C.; Allouche, A. *J. Chem. Phys.* **2001**, *114*, 4226.
(11) Picaud, S.; Toubin, C.; Girardet, C. *Surf. Sci.* **2000**, *103*, 178.
(12) Bussolin, G.; Casassa, S.; Pisani, C.; Ugliengo, P. *J. Chem. Phys.* **1998**, *108*, 9516.
(13) Honrath, R. E.; Peterson, M. C.; Guo, S.; Dibb, J. E.; Shepson, P. B.; Campbell, B. *Geophys. Res. Lett.* **1999**, *26*, 695.
(14) Honrath, R. E.; Guo, S.; Peterson, M. C.; Diiobak, M. P.; Dibb, J. E.; Arsenault, M. A. *J. Geophys. Res.* **2000**, *105*, 24183.
(15) Hudson, R. L.; Moore, M. H. *J. Geophys. Res.-Planet* **2001**, *106 (E12)*, 33275.
(16) Banham, S. F.; Horn, A. B.; Koch, T. G.; Sodeau, J. R. *Faraday Discuss.* **1995**, *100*, 3121.
(17) Graham, J. D.; Roberts, J. T. *J. Phys. Chem. B* **2000**, *104*, 978.
(18) Donsig, H. A.; Herridge, D.; Vickerman, J. C. *J. Phys. Chem. A* **1998**, *102*, 2302.
(19) Horn, A. B.; Chesters, M. A.; McCoustra, M. R. S.; Sodeau, J. R. *J. Chem. Soc. Faraday* Trans. **1992**, *88*, 1077.
(20) Yabushita, A.; Inoue, Y.; Senga, T.; Kawasaki, M.; Sato, S. *J. Phys. Chem. B* **2002**, *106*, 3151.
(21) Kawasaki, M. *Appl. Surf. Sci.* **1998**, *135*, 1159.
(22) Kimmel, G. A.; Stevenson, K. P.; Dohnálek, Z.; Smith, R. S.; Kay, B. D. *J. Chem. Phys.* **2001**, *114*, 5284.
(23) Kimmel, G. A.; Dohnálek, Z.; Stevenson, K. P.; Smith, R. S.; Kay, B. D. *J. Chem. Phys.* **2001**, *114*, 5295.
(24) Stevenson, K. P.; Kimmel, G. A.; Dohnálek, Z.; Smith, R. S.; Kay, B. D. *Science* **1999**, *283*, 1505.
(25) Sato, S.; Yamaguchi, D.; Nakagawa, K.; Inoue, Y.; Yabushita, A.; Kawasaki, M. *Langmuir* **2000**, *16*, 9533.
(26) Regan, P. M.; Langford, S. R.; Ascenzi, D.; Cook, P. A.; Orr-Ewing, A. J.; Ashfold, M. N. R. *Phys. Chem. Chem. Phys.* **1999**, *1*, 3247.
(27) Zimmermann, F. M.; Ho, W. *Surf. Sci. Rep.* **1995**, *22*, 127.
(28) Giorgi, J. B.; Naumkin, F. Y.; Polanyi, J. C.; Raspopov, S. A.; Sze, N. S.-K. *J. Chem. Phys.* **2000**, *112*, 9569.
(29) Samartzis, P. C.; Bakker, B. L.; Rakitzis, T. P.; Parker, D. H.; Kitsopoulos, T. N. *J. Chem. Phys.* **1999**, *110*, 5201.
(30) Zhou, X.-L.; Zhu, X.-Y.; White, J. M. *Surf. Sci. Rep.* **1991**, *13*, 73.
(31) Leutwyler, S. *Nature* **2002**, *417*, 230.
(32) Devlin, J. P.; Uras, N.; Sadlej, J.; Buch, V. *Nature* **2002**, *417*, 269.
(33) Vakarin, E. V.; Badiali, J. P. *Surf. Sci.* **2002**, *513*, 431.
(34) Buch, V.; Sadlej, J.; Uras, N.; Devlin, J. P. *J. Phys. Chem. A* **2002**, *106*, 9374.
(35) Felder, P.; Demuth, C. *Chem. Phys. Lett.* **1993**, *208*, 21.
(36) Yen, M.-W.; Johnson, P. M.; White, M. G. *J. Chem. Phys.* **1993**, *99*, 126.
(37) Polanyi, J. C.; Sze, N. S.-K.; Wang, J.-X. *J. Phys. Chem. A* **1997**, *101*, 6679.
(38) Matsumi, Y.; Tonokura, K.; Kawasaki, M.; Inoue, G.; Satyapal, S.; Bersohn, R. *J. Chem. Phys.* **1991**, *94*, 2669; **1992**, *97*, 5261.
(39) Lide, D. R.; Freerikse, H. P. R. *CRC Handbook of Chemistry and Physics*, 76th ed.; CRC Press: Boca Raton, FL, 1995.
(40) Warner, M. J.; Weiss, R. F. *Deep-Sea Res.* **1985**, *32*, 1485.
(41) Geiger, F. M.; Hicks, J. M.; de Dois, A. C. *J. Phys. Chem. A* **1998**, *102*, 1514.
(42) R. Bianco calculated the structure of $2Cl_2$ and $13H_2O$ at the MP2 level, using effective core potentials for all the heavy atoms. (Private communication.)
(43) Liu, Z. F.; Siu, C. K.; Tse, J. S. *Chem. Phys. Lett.* **1999**, *311*, 93.
(44) Sadtchenko, V.; Knutsen, K.; Giese, C. F.; Gentry, W. R. *J. Phys. Chem. B* **2000**, *104*, 2511.
(45) Alexander, A. J.; Kim, Z. H.; Kandel, S. A.; Zare, R. N.; Rakitzis, T. P.; Asano, Y.; Yabushita, S. *J. Chem. Phys.* **2000**, *113*, 9022.
(46) Singer, S. J.; Freed, K. F.; Band, Y. B. *Adv. Chem. Phys.* **1985**, *61*, 1.
(47) Asano, Y.; Yabushita, S. *J. Phys. Chem. A* **2001**, *105*, 9873.
(48) Bracker, A. S.; Wouters, E. R.; McCoustra, M. R. S.; Suits, A. G.; Vasyutinskii, O. S. *J. Chem. Phys.* **1999**, *110*, 6749.
(49) Johnsson, K.; Engdahl, A.; Ouis, P.; Nelander, B. *J. Phys. Chem.* **1992**, *96*, 5778.